NANO LETTERS

2005
Vol. 5, No. 12
2443−2447

Resonant Coupling between Surface Vibrations and Electronic States in Silicon Nanocrystals at the Strong Confinement Regime

A. Sa'ar,* Y. Reichman, M. Dovrat, D. Krapf,† J. Jedrzejewski, and I. Balberg

Racah Institute of Physics and the Center for Nanoscience and Nanotechnology, The Hebrew University of Jerusalem, Jerusalem 91904, Israel

Received August 31, 2005; Revised Manuscript Received October 10, 2005

ABSTRACT

A striking correlation between infrared photoinduced absorption spectra and the photoluminescence from silicon nanocrystals indicates that quantized electronic sublevels of the nanocrystals are resonantly coupled to surface vibrational modes via a polarization field produced by coherent longitudinal polar vibrations. Our experimental results and model support the assumption that the mechanism responsible for the efficient photoluminescence from silicon nanocrystals should be assigned to inhibition of nonradiative channels rather than enhancement of radiative channels.

The current interest in the optical properties of silicon nanocrystals (nc's) is driven by both fundamental questions concerning the origin of the photoluminescence (PL) from these nc's[1−3] as well as the possibility to develop silicon-based optoelectronic devices.[4,5] Canham[6] in his pioneering work on porous silicon (PS) suggested that quantum confinement (QC) of carriers in small silicon nc's is responsible for the strong, room temperature PL from PS. However, shortly after, numerous models that do not rely on QC were proposed including surface states, surface hydrides, local defects, and molecular species.[1−3,7] At present, there is a general agreement that QC is responsible for the significant blue shift of the PL due to the increase of the energy band gap with the decreasing size of the nanocrystals. Wolkin et al.[8] have argued that the presence of Si═O surface bonds produces localized states in the PS medium that trap electrons thus explaining the pinning of the PL emission from aged PS samples. However, while this and related models[9,10] may account for the energetic dependence of the PL, they do not provide an explanation to the origin of the efficient PL emission from these nc's.

In a recent work[11,12] we have shown that the PL emission from silicon nc's (embedded in a SiO_2 matrix) at temperatures above 40−50 K is dominated by radiative transitions. This conclusion is further supported by recent experiments[13,14] where the PL efficiency at room temperature was found to be of the order of ~1. These experiments and others[15] have shown that radiative transitions from the upper state of the confined exciton in these nc's[16] dominate over nonradiative transitions. Yet, the measured oscillator strength of these radiative transitions has been found to be 3−4 orders of magnitudes *weaker* than the oscillator strength associated with interband optical transitions in direct gap semiconductors.[11−12] As a result, we have concluded that the mechanism that is responsible for the efficient PL from silicon nc's should be assigned to the *exclusion* of nonradiative channels.[11,17] However, to date no such mechanism that would give rise to the exclusion of nonradiative channels in silicon nc's has been proposed or investigated.

One of the most intriguing results concerning this conclusion arises from a comparison of nonradiative lifetimes measured for silicon nc's to that of bulk silicon crystals. The measured nonradiative lifetime from silicon nc's, prepared by a variety of techniques, is in the milliseconds range and is comparable to that measured for highly pure and uniform bulk silicon crystals with a very low density of defects and imperfections.[18] Considering the presence of the high density of defects, the surface area, and the inhomogeneities that characterize silicon nc samples, one would expect significantly faster nonradiative relaxation rates. The present Letter is focused on this question, i.e., a mechanism that can exclude nonradiative processes in silicon nc's. Understanding of this mechanism is expected *not only to explain the origin of the strong PL from silicon nc's but also to advance novel*

* Corresponding author. E-mail: saar@vms.huji.ac.il.
† Present address: Delft University of Technology, Delft, The Netherlands.

10.1021/nl051740e CCC: $30.25 © 2005 American Chemical Society
Published on Web 11/18/2005

conceptions concerning nonradiative processes in strongly confined nanostructures.

In this Letter we argue that the exclusion of nonradiative channels in silicon nc's is due to resonant coupling between surface vibrations and "bulk" electronic states of the silicon nc's. The surface vibrational modes[19] that are coupled to the electronic states are "longitudinal" polar vibrations such as those constructed by Si−O−Si surface bonds,[2,20] which produce a polarization field in the vicinity of the nanocrystals. In close analogy to the polaron problem in polar semiconductors,[21] the polarization field couples polar surface vibrations to the electronic states of the nc's to form a new set of coupled states that we name "vibrons". Using photoinduced infrared absorption (PIA) spectroscopy,[22] we show that in small silicon nc's there is a strong, resonant coupling between surface vibrations and electronic states that forms long-lived vibrons. Hence, in this regime, *surface vibrations do not act as scattering centers* that enhance nonradiative relaxation channels but rather give rise to new coupled states that *eliminate* nonradiative channels. Our model provides a simple and elegant explanation for many intriguing experimental results related to silicon nc's that seem to contradict each other.[1−3] In addition, our experiments and model support the conclusion that the efficient PL from silicon nc's is mainly due to exclusion of nonradiative channels rather than efficient radiative transitions.[11,15]

The samples used for our experiments are silicon nc's embedded in a silicon dioxide (SiO_2) matrix that were fabricated by a cosputtering technique described in refs 11 and 12. This technique allows us to produce a set of samples, each of which is characterized by a given *volume content* of silicon denoted by x,[11−12] which are controlled by the deposition rate of silicon and SiO_2. Silicon nc's are created after 60 min of annealing in nitrogen at a temperature of 1150 °C. A cross-section view of a transmission electron microscopy (TEM) micrograph of the $x = 15\%$ sample and the size distribution of the nc's are shown in Figure 1. The average diameter of the nc's for this sample is ∼4.5 nm with a full width at half-maximum (FWHM) of about 2 nm; see inset to Figure 1. Similar analysis for the other samples has shown that the average diameter of the nc's increases monotonically with x as exhibited by the upper and the lower scales of Figure 2. For example, for the $x \cong 12\%$ sample we find the average diameter to be $d \cong 3 \pm 1$ nm, while for $x \cong 31\%$ we find $d \cong 6.5 \pm 2.5$ nm. PL spectra, taken at room temperature, of samples with varying content of silicon nc's are shown at the inset to Figure 2a while the variation of the PL peak energy and the integrated PL (e.g., the area below each of PL spectra shown at the inset to Figure 2a) versus x are shown in Figure 2a and Figure 2b, respectively. Notice the monotonic red shift of the PL energy with the increasing average size of the crystallites (and x) as expected from the QC model.

Linear infrared (IR) and PIA absorption spectra were measured by the following setup.[22,23] An Ar^+ ion laser operating at 488 nm serves as a pump beam to excite electron−hole pairs (excitons) in the nc's while an IR probe beam of a blackbody source has been used to measure IR absorption spectra. For linear-IR absorption measurements the IR probe beam was modulated by a mechanical chopper while for PIA measurements the pump laser was modulated to yield, PIA = $\Delta T/T$ (with T and ΔT being the linear and the photoinduced transmittance, respectively). Typical linear and PIA spectra for the $x \cong 15\%$ sample are shown in Figure 3. The linear absorption spectrum consists of an asymmetric absorption line at 130−140 meV that is related to the Si−O−Si stretching modes of vibration.[2,20] We would like to emphasize that similar spectra were obtained for all cosputtered samples under investigation. The PIA spectrum reveals two absorption lines, a narrow low-energy line at 135 meV and a broader high-energy line at about 280 meV. We assign

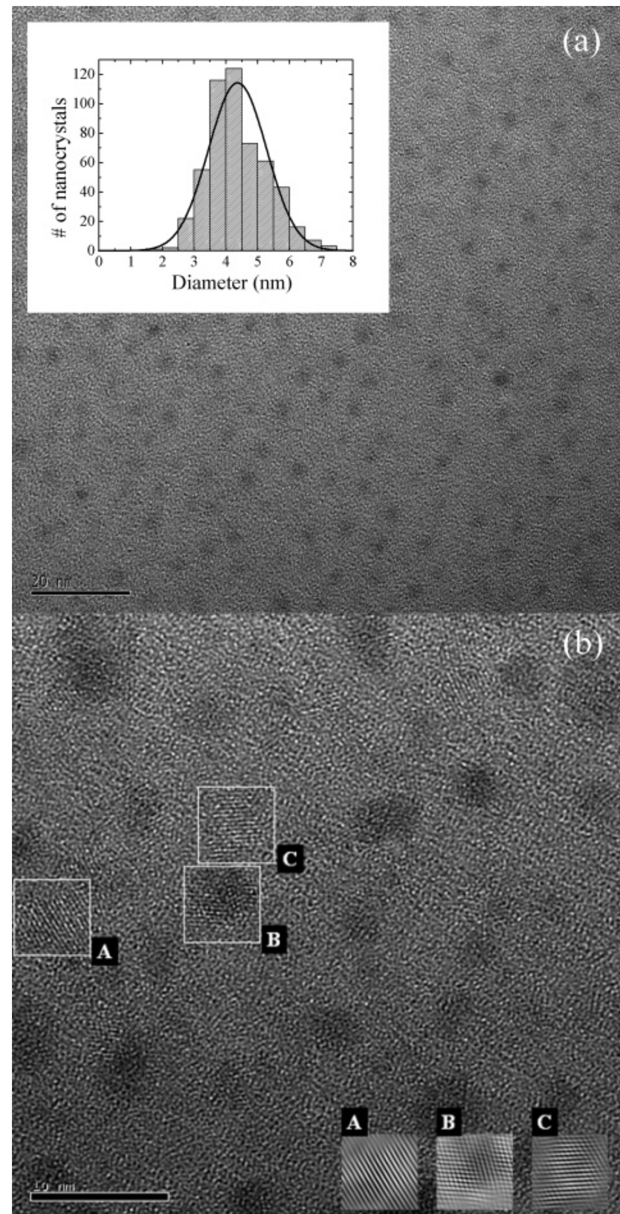

Figure 1. (a) Cross-section view of a high-resolution TEM micrograph revealing silicon nanocrystals in the $x \approx 15\%$ (silicon volume content) sample. The inset is a histogram showing the size distribution of silicon nc's as determined from TEM images. (b) A higher magnification image where the insets A, B, and C reveal silicon crystal planes (after filtering in the frequency domain) of those nanocrystals marked by squares.

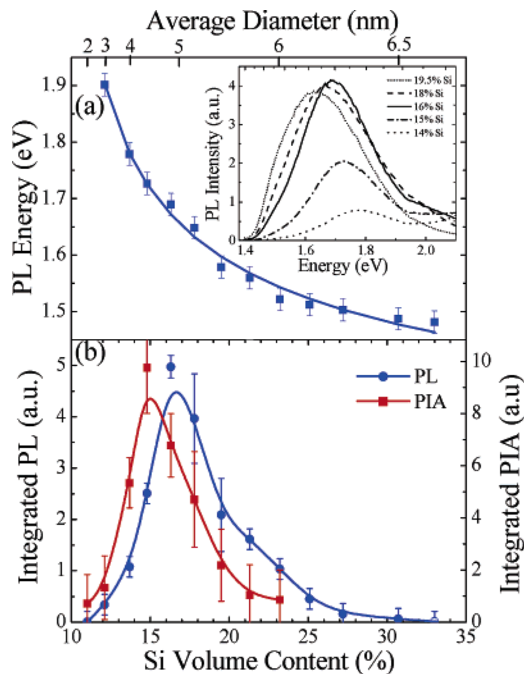

Figure 2. (a) The energy of the PL peak versus both the average silicon volume content (lower x axis) and the average diameter of the nanocrystals (top x axis). The inset shows typical PL spectra of the samples. (b) The integrated PL (blue circles) and the integrated PIA (red squares) versus the silicon volume content.

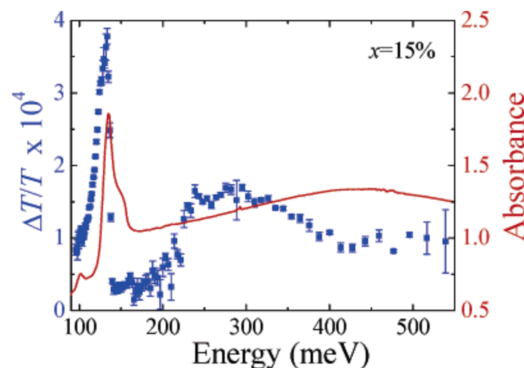

Figure 3. Room-temperature PIA (blue squares) and linear (red line) IR absorption spectra for the $x = 15\%$ (silicon volume content) sample.

the low-energy and the high-energy lines to valence intersublevel (ISL) and conduction ISL optical transitions, respectively. This assignment (see below) is based on a simple effective mass model,[24] as our experimental technique is not sensitive to the polarity of the carriers. In addition, one can observe a sharp cutoff of the valence-ISL absorption line at about 135 meV that is correlated with the Si−O−Si vibration energy.

Next, in Figure 4 we show PIA spectra for samples with varying silicon content, x. It is evident that the two PIA lines appear for all samples. However, while the high-energy peak of the conduction ISL shows a remarkable red shift with the increasing size of the nc's, the low-energy peak of the valence ISL shows a significantly weaker shift. In addition, one can see that the PIA spectra decrease in amplitude with the increasing size of the nc's and cannot be revealed for x > 25%. In contrast, we found that for all samples the linear Si−O−Si vibration spectrum has essentially the same magnitude and shape. These results indicate that the origin of the PIA lines should be assigned *not* to pure vibrational modes but rather to electronic ISL transitions induced by the pump laser. The cutoff energy at ∼135 meV could be revealed for most samples except the high-x samples where the valence-ISL line is red shifted to lower energies.

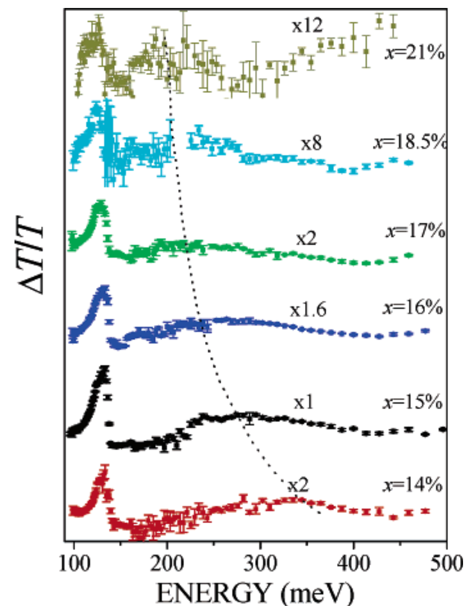

Figure 4. PIA spectra for various samples of different silicon volume content. The dashed line indicates the remarkable red shift of the high-energy ISL line with the increasing size of the nc's.

To further analyze the PIA spectra of Figure 4, we show in Figure 5 the PIA spectral peak energies vs the confinement energy, $\Delta E = E_{PL} - E_G$, where E_{PL} is the PL peak energy and $E_G \cong 1.1$ eV is the energy gap of a bulk silicon crystal. It can be seen that the conduction-ISL peak energies display a linear dependence on ΔE as can be expected from a simple QC model, i.e., both ΔE and ΔE_{CISL} monotonically increase, in the same proportion, with the decreasing size of the nc's. On the other hand, the valence-ISL peak energies show a sublinear dependence on ΔE approaching very rapidly an asymptotic value very close to that of the Si−O−Si vibrational energy (shown by the horizontal dashed line in Figure 5b). The results shown in Figure 5b suggest that the quantized electronic states of the nc's are coupled to surface vibrations. To follow this argument, we have drawn in Figure 5b a straight (dotted) line that, as explained above, represents the expected behavior of the valence ISL according to the QC model. This line and the horizontal dashed line of the Si−O−Si vibration (that is independent of the nc's size) cross each other. The anticrossing behavior found in our experiments suggests that *the electronic states and the vibrations are coupled*.

Turning now to the mechanism that can couple the abovementioned states, we illustrate in Figure 6 a simple model for the structure of a silicon nc that is terminated by Si−O surface bonds. The vibration at ∼135 meV, schematically illustrated at the bottom of Figure 6, is related to a stretching

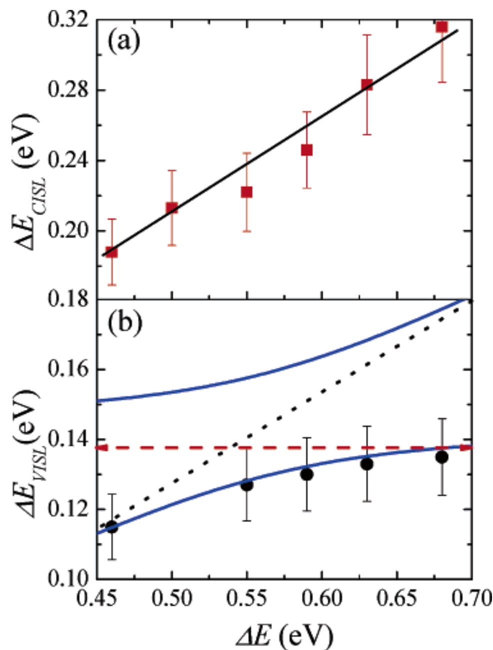

Figure 5. (a) The measured conduction-ISL peak photon energies. The black solid line represents a linear dependence of the conduction-ISL energies on the confinement energy. (b) The valence-ISL energies vs the confiment energy. The curves (blue lines) are obtained by fitting the vibron's model to the experimental data. The horizontal red dashed line indicates the Si−O−Si vibrational energy while the black dotted line indicates the QC model's prediction for valence-ISL transitions.

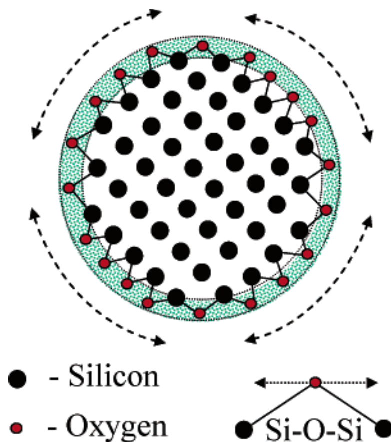

Figure 6. Schematic illustration of a silicon nanocrystal terminated with silicon−oxygen bonds. The dashed area stands for a surface region where crystalline SiO_2 can be formed to allow longitudinal surface polar vibrations. The inset schematically illustrates the Si−O−Si stretching mode of vibration.

mode of vibrations where the oxygen atom vibrates in the Si−O−Si plane parallel to the line joining the two silicon atoms.[20] We propose that this polar vibration,[25] which produces a "longitudinal" polarization field,[26] is strongly coupled to the quantized electronic states of the nc's by the polarization field.[7] While we do not attempt to evaluate the actual modes of vibration on the surface of small silicon nc's, we note that it has been argued that such an interface includes a few monolayers of crystalline SiO_2[9] (for example, in the form of tridymite[27] or cristobalite[28]). This type of surface can give rise to coherent vibrations across the surface and a generation of a remarkable polarization field. Hence, in analogy to polarons in polar semiconductor nanostructures,[21,29] the polarization field produces a strong, resonant mixing between the nc electronic states and surface vibrations once the energy separation between the electronic states and the vibrational energy becomes comparable. Notice also that bulk silicon is *not* a polar semiconductor and, therefore, bulk and quantized phonons of silicon cannot be coupled to the electronic states. To follow the vibrons behavior, we have used a semiquantitative model such as those used for similar many-body problems.[21] We present the frequency-dependent dielectric function of the vibron as

$$\epsilon(\omega)/\epsilon = \frac{\Omega_{\mathrm{VISL}}^2}{\omega_{\mathrm{VISL}}^2 - \omega^2 - i\gamma_{\mathrm{VISL}}\omega} + \frac{\Omega_{\mathrm{V}}^2}{\omega_{\mathrm{V}}^2 - \omega^2 - i\gamma_{\mathrm{V}}\omega} + 1 \tag{1}$$

where the first term in eq 1 stands for the contribution of electronic valence ISL transitions[30,31] and the second term stands for the contribution of surface vibrations to the total dielectric function; Ω_{V} and Ω_{VISL} are coupling strengths for vibrations and valence ISL, respectively, and $h\omega_{\mathrm{V}}$ and $h\omega_{\mathrm{VISL}}$ are the resonant vibration and ISL energies. To first-order approximation, the solution of the vibron problem is obtained by finding the poles of $1/\epsilon(\omega)$, e.g., by setting the real part of $\epsilon(\omega)$ to zero.[32] The solutions are shown by the solid lines in Figure 5b. Here, we took Ω_{VISL} to be a free parameter that is extracted from the fitting. It is important to note that when dealing with one- and two-dimensional nanostructures (i.e., quantum wires and wells) one usually takes Ω_{VISL} to be the plasma frequency describing a collective motion of the carriers. Obviously, this simple picture cannot be applied to small silicon nc's as our vibron system is more similar to excitonic polarons in quantum dots.[33] Nevertheless, despite the simplicity of the model, the agreement with the experimental results is evident. Notice also that our model provides a simple explanation to the strong correlation between the integrated PL and PIA shown in Figure 2b. This suggests that the same mechanism, e.g., formation of vibrons, dominates for both types of optical transitions. The long-lived vibrons give rise to slow nonradiative relaxation rates that, in turn, enhance the PL efficiency. Both the PL and the PIA approach a maximum of emission/absorption for the sample where the (average) diameter of the nc is ∼4.5 nm. For this diameter we find the energy of vibration to coincide with the ISL electronic energy. Finally, we notice that one may argue that the two groups of PIA lines (see Figure 4) are related to ISL transitions associated with only one of the carriers and that the splitting takes place due to coupling to surface vibrations. On the basis of our current analysis and experimental results, we cannot rule out this possibility. However, this will not modify any of our conclusions regarding the nature of the coupling mechanism.

In conclusion, using infrared PIA spectroscopy of silicon nc's with varying sizes, we were able to resolve two groups of ISL transitions. While the high-energy conduction-ISL transitions follow the QC model and linearly increase with the increasing confinement energy, the valence-ISL transi-

tions show a sub-linear dependence on the confinement energy approaching the vibrational energy of the Si−O−Si bonds. The anticrossing behavior of the valence ISL and the vibration energies indicates that the electronic states of the nc's are coupled to surface vibrations to form long-lived vibrons. We suggest that the coupling mechanism is due to a polarization field produced by coherent longitudinal surface vibrations. Our model provides a simple explanation to many intriguing results related to discrepancies between the QC and the surface states models. For example, the possibility of having self-trapping surface states reported by Wolkin et al.[8] and in refs 34−37 as well as the observation of trapped charges reported by Ng et al.[38] are all consistent with our vibron's picture.

Acknowledgment. This work was supported by the Israel Science Foundation (ISF), by the Israeli Ministry of Science, and by Intel Corporation. We thank Dr. Inna Popov from the Hebrew University Center for Nanoscience and Nanotechnology for the TEM analysis.

References

(1) Cullis, A. G.; et al. *J. Appl. Phys.* **1997**, *82*, 909.
(2) Theiss, W. *Surf. Sci. Rep.* **1997**, *29*, 91.
(3) For a collection of reviews see: *Light Emission in Silicon*: *From Physics to Devices*; Lockwood, D. J., Ed.; Academic: New York, 1998. Bisi, O.; et al. *Surf. Sci. Rep.* **2000**, *38*, 1.
(4) Koshida, N.; Matsumoto, N. *Mater. Sci. Eng.* **2003**, R*40*, 169. Pavesi, L.; et al. *Appl. Phys. Lett.* **1995**, *67*, 3280.
(5) Givant, A.; et al. *Appl. Phys. Lett.* **1998**, *73*, 3150. Ben-Tabou de-Leon, S.; et al. *Appl. Phys. Lett.* **2004**, *84*, 4361.
(6) Canham, L. T. *Appl. Phys. Lett.* **1990**, *57*, 1046.
(7) Mason, M. D.; et al. *Phys. Rev. Lett.* **1998**, *80*, 5405.
(8) Wolkin, M. V.; et al. *Phys. Rev. Lett.* **1999**, *82*, 197.
(9) Daldosso, N.; et al. *Phys. Rev. B* **2003**, *68*, 085327.
(10) Puzder, A.; et al. *Phys. Rev. Lett.* **2002**, *88*, 097401. Garrido, B.; et al. *Appl. Phys. Lett.* **2000**, *77*, 3143. Wu, X. L. *Phys. Rev. B* **2000**, *62*, R7759. Vasiliev, I.; et al. *Phys. Rev. B* **2002**, *65*, 121302. Xue, F.-S.; et al. *J. Appl. Phys.* **1997**, *81*, 3175. Luppi, M.; et al. *J. Appl. Phys.* **2003**, *94*, 2130.
(11) Dovrat, M.; et al. *Phys. Rev. B* **2004**, *69*, 155311.
(12) Dovrat, M.; et al. *Phys. Status Solidi C* **2005**, *2*, 3440.
(13) Ledoux, G.; et al. *Phys. Rev. B* **2000**, *62*, 15942.
(14) Lopez, M.; et al. *Solid State Electron.* **2001**, *45*, 1495.
(15) Garcia, G.; et al. *Physica E* **2003**, *16*, 429.
(16) Diener, J.; et al. *Appl. Phys. Lett.* **1999**, *74*, 3350.
(17) Tsybeskov, L.; et al. *Appl. Phys. Lett.* **1999**, *75*, 2265; *Appl. Phys. Lett.* **1998**, *72*, 43.
(18) Sze, S. M. *Physics of Semiconductor Devices*, 2nd ed.; Wiley-Interscience: New York, 1981.
(19) Kanemitsu, Y.; et al. *Phys. Rev. B* **1996**, *54*, 14329.
(20) Lucovsky, G.; et al. *Phys. Rev. B* **1983**, *28*, 3225.
(21) Mahan, G. D. *Many-Particle Physics*, 3rd ed.; Kluwer: New York, 2000.
(22) See for example: Krapf, D.; et al. *Phys. Rev. B* **2004**, *69*, 073301. Calderon, S.; et al. *Phys. Rev. B* **2000**, *62*, 9935.
(23) Krapf, D.; et al., *Phys. Status Solidi A* **2003**, *197*, 566.
(24) Efros, Al. L.; Rosen, M. *Annu. Rev. Mater. Sci.* **2000**, *30*, 475.
(25) Lu, J.-Q.; Koch, F. *Microelecron. Eng.* **1999**, *48*, 95. Hess, K.; Vogl, P. *Solid State Commun.* **1979**, *30*, 797.
(26) The term "longitudinal" polarization field should be understood in the context that the vibrational modes produce dipoles that are directed essentially parallel to the surface of the nc's. We did not observe similar PIA spectra for other vibrations of the Si−O−Si bonds where the oxygen atoms vibrate perpendicular to the Si−Si surface plane.
(27) Ourmazd, A.; et al. *Phys. Rev. Lett.* **1987**, *59*, 213.
(28) Kageshima, H.; Shiraishi, K. *Surf. Sci.* **1997**, *380*, 61.
(29) Mooradian, A.; McWhorter, A. L. *Phys. Rev. Lett.* **1967**, *19*, 849.
(30) Hameau, S.; et al. *Phys. Rev. Lett.* **1997**, *83*, 4152.
(31) Liu, H. C.; et al. *Phys. Rev. Lett.* **2003**, *90*, 77402.
(32) See ref 21, pages 467−475 for a similar treatment for heavily doped semiconductors.
(33) Verzelen, O.; et al. *Phys. Rev. Lett.* **2002**, *88*, 146803.
(34) Cichos, F.; et al. *Phys. Rev. B* **2004**, *70*, 115314.
(35) Hadjisavvas, G.; Kelires, P. C. *Phys. Rev. Lett.* **2004**, *93*, 226104.
(36) Biteen, J. S.; et al. *Appl. Phys. Lett.* **2004**, *84*, 5389.
(37) Khriachtchev, L.; et al. *Appl. Phys. Lett.* **2004**, *85*, 1511.
(38) Ng, C. Y.; et al. *Appl. Phys. Lett.* **2004**, *85*, 2941.

NL051740E